ELECTRONIC SUPPLEMENTARY INFORMATION

Raising of the effective energy barrier promoted by the change of counteranion in a Zn-Dy-Zn SMM: Slow relaxation via the second excited state

I. Oyarzabal, J. Ruiz, E. Ruiz, D. Aravena, E. Colacio and J. M. Seco

Synthetic procedures

All reagents were obtained from commercial sources and used as received. The ligand H_2L (N,N'-dimethyl-N,N'-bis(2-hidroxy-3-formyl-5-bromo-benzyl)ethylenediamine) was prepared following a reported procedure.[1]

(1) M. Yonemura, Y. Matsumura, M. Ohba, H. Okawa and D. E. Fenton, *Chem. Lett*. 1996, 601.

Synthesis of 1

To a solution of $ZnCl_2$ (8.5 mg, 0.0625 mmol) in 5 mL of MeOH were subsequently added with continuous stirring 64 mg (0.125 mmol) of H_2L, 27.4 mg (0.0625 mmol) of $Dy(NO_3)_3 \cdot 5H_2O$ and 23 mg (0.125 mmol) of KPF_6. The resulting solution was filtered and allowed to stand at room temperature. After several days, well-formed prismatic yellow crystals of **1** were obtained, which were filtered off and dried in vacuum. Yield: 19%. Anal. Calcd. for $C_{40}H_{40}N_4O_8Br_4Cl_2PF_6DyZn_2$: C, 31.33; H, 2.63; N, 3.65. Found: C, 31.51; H, 2.67; N, 3.72.

Physical measurements

Elemental (C, H, and N) analyses were performed on a Leco CHNS-932 microanalyzer. IR spectra of powdered samples were recorded in the 400-4000 cm^{-1} region on a Nicolet 6700 FTIR spectrophotometer using KBr pellets. Variable-temperature magnetic susceptibility (2-300 K) and magnetization measurements at 2 K and different magnetic fields (0-50 kOe) were carried out with a Quantum Design SQUID MPMS XL5 magnetometer. Diamagnetic corrections were estimated from the Pascal´s constants. Alternating current magnetic measurements in a 3.5 G ac field were performed on a PPMS (Physical Property measurement System) - Quantum Design Model 6000.

Crystallographic data and Refinement

X-ray crystal data for **1** were collected with an Agilent Technologies Super-Nova diffractometer, which was equipped with monochromated Mo Kα radiation ($\lambda = 0.71069$ Å) and Eos CCD detector. Data frames were processed (unit cell determinations, intensity data integrations, routine corrections for Lorentz and polarization effects and analytical absorption corrections) using the CrysAlis Pro software package.[2] The structures were solved by direct methods and refined by full-matrix least-squares with SHELXL-97.[3]

Final $R(F)$, w$R(F^2)$ and goodness of fit agreement factors, details of the data collection and analysis can be found in Table S1. Selected bond lengths and angles are given in Table S2.

(2) *CrysAlisPro Software System*, Agilent Technologies UK Ltd, Oxford, UK, 2012.

(3) G. M. Sheldrick, *Acta Crystallogr., Sect. A: Fundam. Crystallogr.*, 2008, **64**, 112.

Table S1.- Crystallographic data for **1**.

Compound	1
Formula	$C_{40}H_{40}Br_4Cl_2DyF_6N_4O_8PZn_2$
M_r	1533.51
Crystal system	Monoclinic
Space group (no.)	*C2/c* (15)
a (Å)	17.1014(2)
b (Å)	18.2552(3)
c (Å)	15.9346(2)
α (°)	90.00
β (°)	97.4595(12)
γ (°)	90.00
V (Å^3)	4932.51(11)
Z	4
D_c (g cm^{-3})	2.065
μ(MoKα) (mm^{-1})	5.921
T (K)	100(2)
Observed reflections	4336 (3679)
R_{int}	0.0393
Parameters	310
GOF	1.048
R_1[a,b]	0.0412 (0.0307)
wR_2[c]	0.0653 (0.0613)
Largest difference in peak and hole (e Å^{-3})	0.891 and -0.540

[a] $R_1 = \Sigma||F_o| - |F_c||/\Sigma|F_o|$.

[b] Values in parentheses for reflections with $I > 2\sigma(I)$.

[c] w$R_2 = \{\Sigma[w(F_o^2 - F_c^2)^2] / \Sigma[w(F_o^2)^2]\}^{1/2}$

Table S2.- Selected bond lengths (Å) and angles (°) for **1**.

Compound	1
Dy(1)-Zn(1)	3.550(1)
Dy(1)-O(1)	2.393(3)
Dy(1)-O(2)	2.340(3)
Dy(1)-O(3)	2.275(3)
Dy(1)-O(4)	2.386(3)
Zn(1)-N(1)	2.153(3)
Zn(1)-N(2)	2.106(3)
Zn(1)-O(2)	2.066(3)
Zn(1)-O(3)	2.138(3)
Zn(1)-Cl(1)	2.217(1)
Dy(1)-O(2)-Zn(1)	107.2(1)
Dy(1)-O(3)-Zn(1)	107.1(1)
Zn(1)-Dy(1)-Zn(1)	109.48(1)
O(1)-Dy(1)-O(2)	71.8(1)
O(1)-Dy(1)-O(4)	77.6(1)
O(2)-Dy(1)-O(3)	68.1(1)
O(3)-Dy(1)-O(4)	73.0(1)
O(2)-Zn(1)-O(3)	75.9(1)
O(2)-Zn(1)-Cl(1)	107.62(9)
O(3)-Zn(1)-Cl(1)	101.78(8)
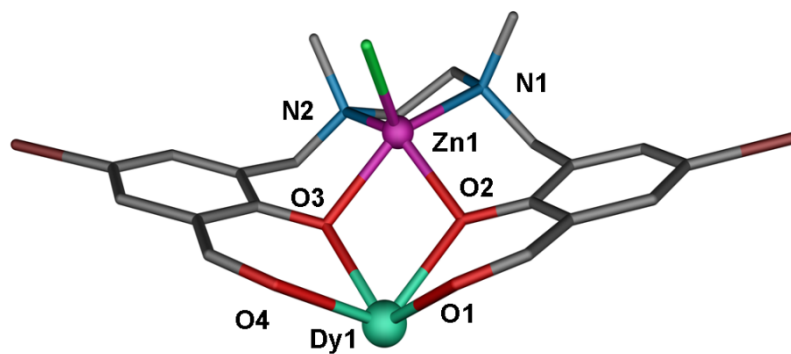
The [ZnCl(L)Dy]$^{2+}$ subunit with the labelling used in Table S2.

Computational details

Low-energy spectra and g factors of the eight lowest Kramers doublets of **1** were obtained by means of CASSCF+RASSI calculations, as implemented in the MOLCAS 7.8 software package.[4] The method is divided in two steps: 1) CASSCF(9,7) calculations for three different multiplicities (sextet, quartet and doublet), 2) The effect of spin–orbit coupling on the basis of the converged wavefunctions obtained in the previous step is included by the restricted active space state interaction (RASSI) method. Spin Hamiltonian parameters (such as g factors) can be calculated from the wavefunctions resulting from the state interaction step employing the SINGLE ANISO program. We included 21, 128 and 98 roots for the sextet, quartet and doublet CASSCF calculations, while the employed basis set has the following contractions: Dy[9s8p6d4f3g2h]; Br [4s3p2d1f]; Zn [4s3p2d1f]; Cl [4s3p1d]; O [4s3p2d1f]; N [4s3p2d1f]; C [3s2p]; H [2s]. The structure of the model was extracted from the corresponding X-ray structure without any ligand truncation. Electrostatic potential maps were obtained by DFT calculations (functional: B3LYP, basis: TZVP, program: Gaussian09),[5] employing the geometry for the ligand environment of the previous CASSCF+RASSI calculations and removing the DyIII ion.

(4) F. Aquilante, L. De Vico, N. Ferré, G. Ghigo, P.-Å. Malmqvist, P. Neogrády, T. B. Pedersen, M. Pitoňák, M. Reiher, B. O. Roos, L. Serrano-Andrés, M. Urban, V. Veryazov and R. J. Lindh, *Comput. Chem.* 2010, **31**, 224.

(5) Gaussian 09, M. J. Frisch, G. W. Trucks, H. B. Schlegel, G. E. Scuseria, M. A. Robb, J. R. Cheeseman, G. Scalmani, V. Barone, B. Mennucci, G. A. Petersson, H. Nakatsuji, M. Caricato, X. Li, H. P. Hratchian, A. F. Izmaylov, J. Bloino, G. Zheng, J. L. Sonnenberg, M. Hada, M. Ehara, K. Toyota, R. Fukuda, J. Hasegawa, M. Ishida, T. Nakajima, Y. Honda, O. Kitao, H. Nakai, T. Vreven, J. A. Montgomery, J. E. Peralta, F. Ogliaro, M. Bearpark, J. J. Heyd, E. Brothers, K. N. Kudin, V. N. Staroverov, R. Kobayashi, J. Normand, K. Raghavachari, A. Rendell, J. C. Burant, S. S. Iyengar, J. Tomasi, M. Cossi, N. Rega, N. J. Millam, M. Klene, J. E. Knox, J. B. Cross, V. Bakken, C. Adamo, J. Jaramillo, R. Gomperts, R. E. Stratmann, O. Yazyev, A. J. Austin, R. Cammi, C. Pomelli, J. W. Ochterski, R. L. Martin, K. Morokuma, V. G. Zakrzewski, G. A. Voth, P. Salvador, J. J. Dannenberg, S. Dapprich, A. D. Daniels, Ö. Farkas, J. B. Foresman, J. V. Ortiz, J. Cioslowski and D. J. Fox, Gaussian: Wallingford, CT, 2009.

Table S3.- Continuous Shape Measures Calculations for LnO_8 coordination environment in compounds **1** and **1 a**

<u>Compound 1</u>

```
OP-8           1 D8h   Octagon
HPY-8          2 C7v   Heptagonal pyramid
HBPY-8         3 D6h   Hexagonal bipyramid
CU-8           4 Oh    Cube
SAPR-8         5 D4d   Square antiprism
TDD-8          6 D2d   Triangular dodecahedron
JGBF-8         7 D2d   Johnson gyrobifastigium J26
JETBPY-8       8 D3h   Johnson elongated triangular bipyramid
J14
JBTPR-8        9 C2v   Biaugmented trigonal prism J50
BTPR-8        10 C2v   Biaugmented trigonal prism
JSD-8         11 D2d   Snub diphenoid J84
TT-8          12 Td    Triakis tetrahedron
ETBPY-8       13 D3h   Elongated trigonal bipyramid
```

<u>Compound **1**</u>

Structure [ML8]	OP-8	HPY-8	HBPY-8
CU-8	SAPR-8	TDD-8	JGBF-8	JETBPY-8
JBTPR-8	BTPR-8	JSD-8	TT-8	ETBPY-8
T14	,	30.192,	23.090,	16.569,
10.538,	<mark>0.547</mark>,	2.870,	15.239,	26.011,
3.365,	2.716,	5.868,	11.334,	21.716

<u>Compound **1a**</u>

ETBPY-8	TT-8	JSD-8	BTPR-8	JBTPR-8	JETBPY-8	JGBF-8
24.742,	8.029,	5.750,	2.862,	3.321,	29.125,	15.237,

TDD-8	SAPR-8	CU-8	HBPY-8	HPY-8	OP-8
2.173,	<mark>0.927</mark>,	7.165,	13.663,	21.555,	31.300

Table S4.- Continuous Shape Measures Calculations for ZnN_2O_2Cl coordination environment in compound **1**.

<u>Compound 1</u>

```
PP-5           1 D5h   Pentagon
vOC-5          2 C4v   Vacant octahedron
TBPY-5         3 D3h   Trigonal bipyramid
SPY-5          4 C4v   Spherical square pyramid
JTBPY-5        5 D3h   Johnson trigonal bipyramid J12
```

Structure [ML5]	PP-5	vOC-5	TBPY-5	SPY-5	JTBPY-5
T14	,	32.506,	3.519,	4.070,	0.678,	7.170
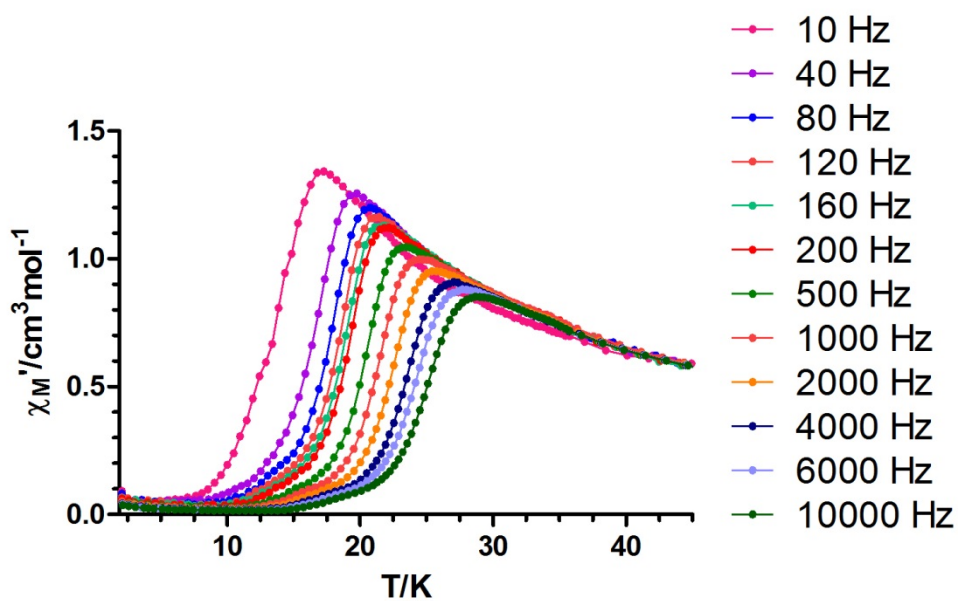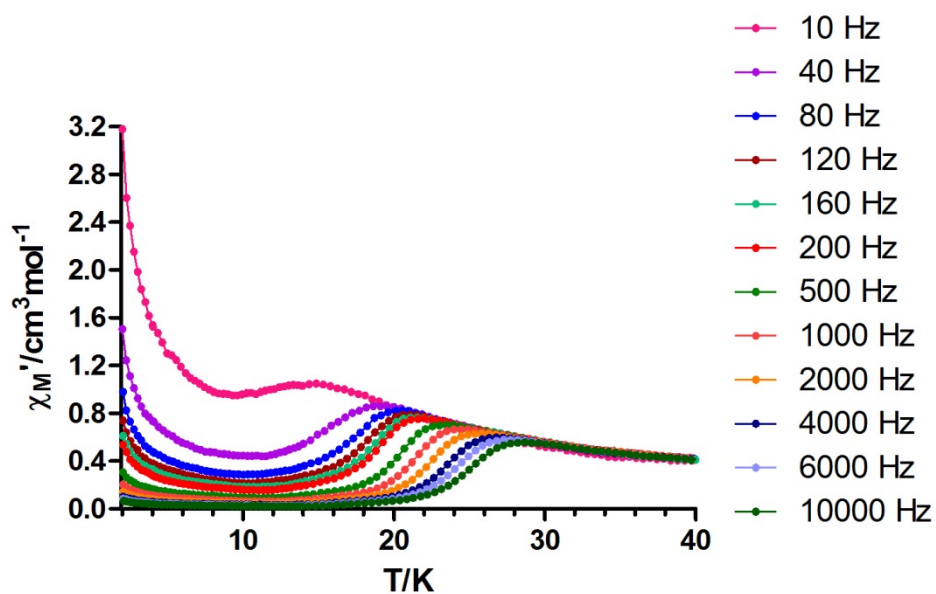
Figure S1.-Temperature dependence of the molar in-phase ac susceptibility (χ_M') for **1** under zero (up) and 1000 Oe (bottom) *dc* applied field at different frequencies.
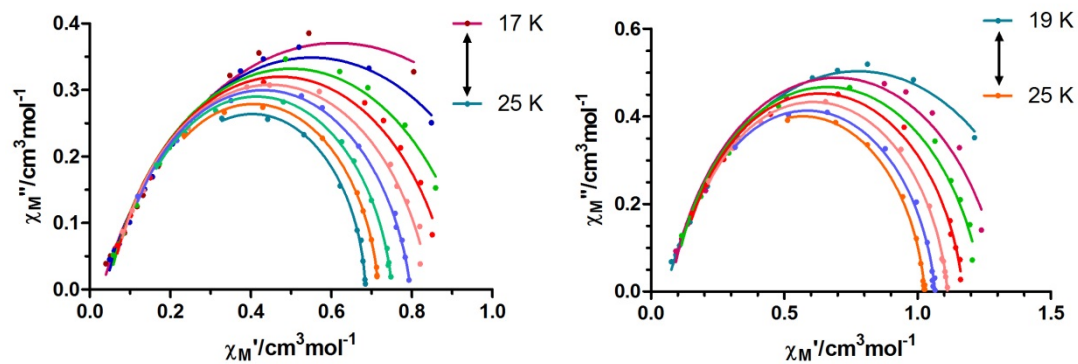
Figure S2.- Cole-Cole plot for **1** under zero (left) and 1000 Oe (right) *dc* applied field at different temperatures.
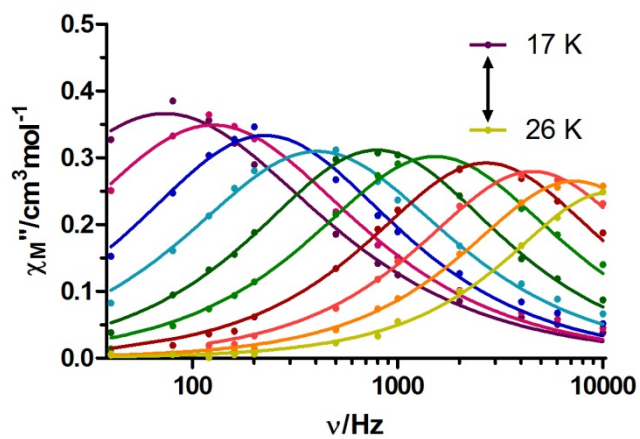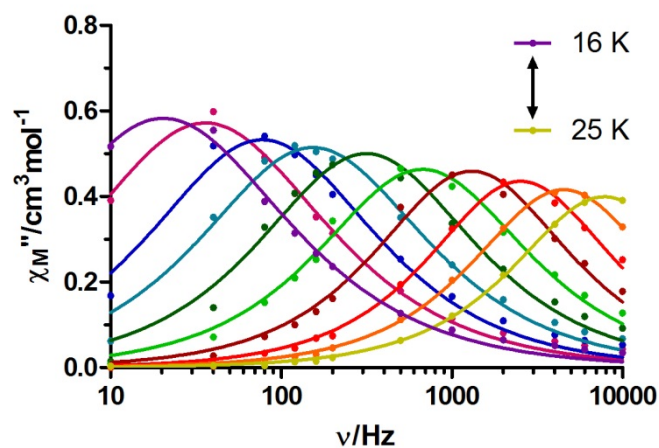
Figure **S3**.-Frequency dependence of the molar out-of-phase ac susceptibility (χ_M'') for **1** under zero (up) and 1000 Oe (bottom) *dc* applied field at different temperatures.

Table **S5.-** Calculated energies (cm^{-1}) and g-factors for the eight lowest Kramers' doublets.

Doublet	Energy (cm^{-1})	g_z	g_y	g_x	Angle wrt. Ground doublet (degrees)
1	0.0	19.636	0.000	0.000	-
2	144.2	16.561	0.045	0.041	2.4
3	243.3	11.630	4.457	1.959	47.5
4	264.7	8.895	3.944	2.703	61.9
5	323.3	6.866	2.722	0.859	14.8
6	347.4	2.488	8.210	11.024	22.7
7	369.2	19.499	0.737	0.428	89.9
8	491.8	19.581	0.002	0.001	53.1
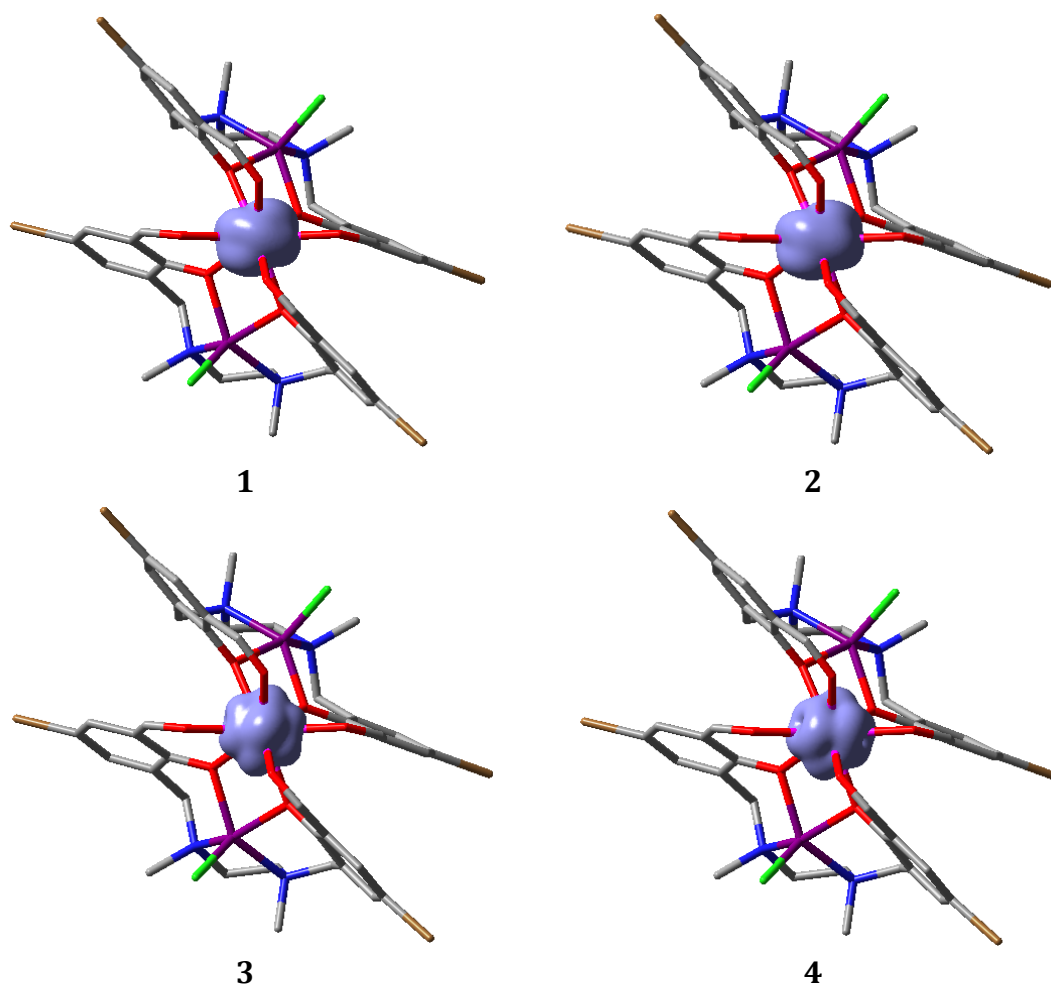
Figure S4.- Beta spin density of the Dy^{III} f electrons for the first 4 non-relativistic states.

Table **S6.-** First excitation energies (cm^{-1}) from the states stemming form the ground ^{6}H term at CASSCF level.

State	Energy (cm^{-1})
1	0.0
2	0.6
3	200.6
4	236.2
5	305.5
6	346.1
7	394.5
8	418.3
9	424.7
10	562.1

[ZnCl(μ-L)Dy(μ-L)ClZn][ZnCl₃(CH₃OH)]
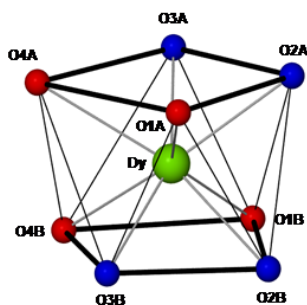
Dy-O(1A) = 2.397(4) Å
Dy-O(2A) = 2.323(5) Å
Dy-O(3A) = 2.253(5) Å
Dy-O(4A) = 2.443(5) Å

Dy-O(1B) = 2.387(4) Å
Dy-O(2B) = 2.349(5) Å
Dy-O(3B) = 2.244(5) Å
Dy-O(4B) = 2.387(5) Å

[ZnCl(μ-L)Dy(μ-L)ClZn]PF₆
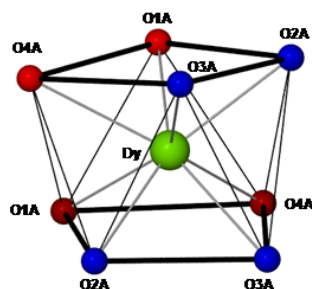
Dy-O(1A) = 2.386(3) Å
Dy-O(2A) = 2.275(3) Å
Dy-O(3A) = 2.340(3) Å
Dy-O(4A) = 2.392(3) Å

Figure S5.- DyO_8 coordination polyhedra for [ZnCl(μ-L)Dy(μ-L)ClZn][ZnCl$_3$(CH$_3$OH)] and [ZnCl(μ-L)Dy(μ-L)ClZn]PF$_6$.
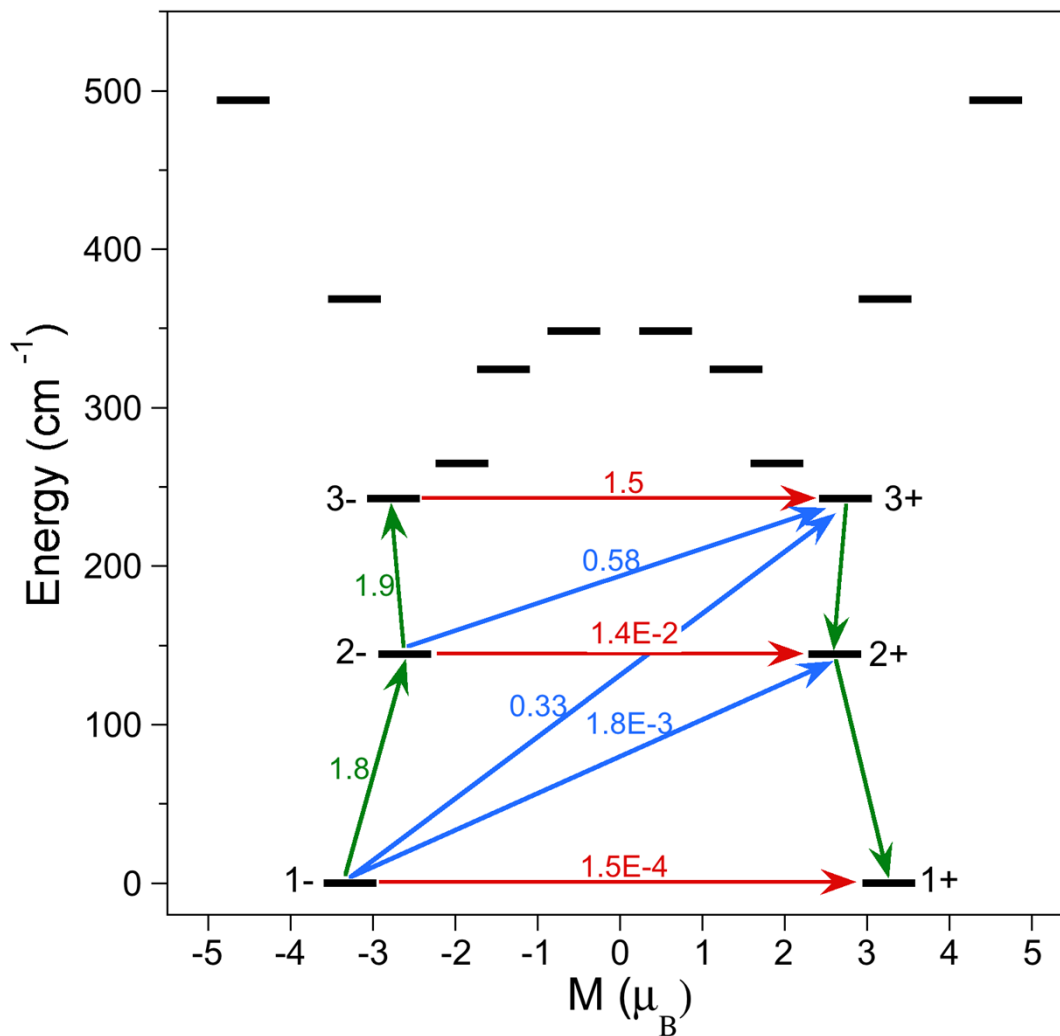
Figure S6.- Eight lowest Kramers doublets (KDs) and *ab initio* computed relaxation mechanism in **1.** The thick black lines imply KDs as a function of their magnetic moment along the main anisotropy axis.The red lines correspond to ground state QTM and TA-QM via the first and second excited KDs, blue lines show possible Orbach relaxation processes. The values indicated close to the arrows indicate the matrix elements of the transition magnetic moments.
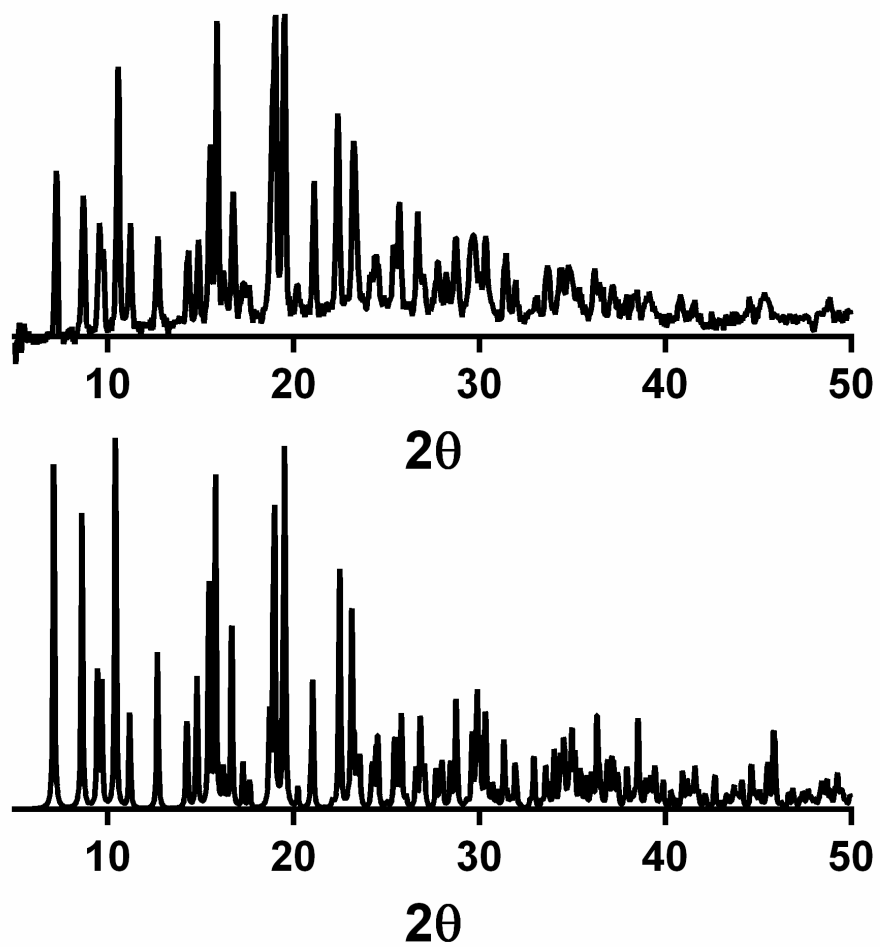
Figure S7. Experimental (top) and simulated (bottom) powder X-ray diffractograms for **1**.